Thermal footprint of an eroded thrust sheet in the southern Appalachian thrust belt, Alabama, USA

William A. Thomas
Department of Earth and Environmental Sciences, University of Kentucky, Lexington, Kentucky 40506-0053, USA

Ravi V.S. Kanda
Division of Geological and Planetary Science, California Institute of Technology, Pasadena, California 91125, USA

Kieran D. O'Hara
D. Matthew Surles*
Department of Earth and Environmental Sciences, University of Kentucky, Lexington, Kentucky 40506-0053, USA

ABSTRACT

Erosion of the leading hanging-wall cutoffs of thrust sheets commonly obscures the magnitude of thrusting. The Jones Valley thrust fault in the southern Appalachian thrust belt in Alabama, USA, is exposed along a northwest-directed, large-scale frontal ramp, and the leading part of the thrust sheet has been eroded. Previously published and newly collected vitrinite reflectance data from Pennsylvanian coal beds document a distinct, northeast-trending, elongate, oval-shaped thermal anomaly northwest of the trace of the Jones Valley fault. The northwest edge of the thermal anomaly is ~18 km northwest of the fault trace, suggesting the original extent of the eroded thrust sheet. The anomaly ends both northeastward and southwestward along strike at lateral ramps. The southeast edge of the anomaly corresponds to the location of a footwall frontal ramp.

A three-dimensional heat conduction model for simultaneous horizontal (two-dimensional) and vertical heat flow in a rectangular thrust sheet is designed to test whether the documented thermal anomaly ($\%R_o$ = 1.0–1.6) may reflect the former extent of thrust-sheet cover. The model uses a 3-km-thick thrust sheet with horizontal dimensions of 10 × 30 km, as well as a three-dimensional analytical solution to the heat conduction equation, whereby the thrust sheet cools both laterally and vertically. The model reproduces the magnitude and oval shape of the vitrinite reflectance anomaly at 100–500 k.y. after thrust emplacement. The geothermal gradient reaches a steady state at ~2 m.y., and is never fully reestablished even for long times because of lateral cooling in the hanging wall.

Thickness and extent of the thrust sheet from the thermal model are consistent with balanced and restored cross sections of the Jones Valley thrust sheet based on geologic data; a thrust sheet ~3 km thick was emplaced ~18 km onto the foreland over the site of the thermal anomaly. The three-dimensional thermal evolution of both the hanging wall and the footwall is distinct from that predicted from one-dimensional models; a three-dimensional model predicts less heating of the footwall because of horizontal heat loss across bounding ramps.

INTRODUCTION

In exposed thrust belts, the leading hanging-wall cutoffs of the thrust sheets commonly have been removed by erosion, and as a result, the magnitude of thrusting is difficult to quantify. Tectonic thickening by thrust imbrication and stacking increases the thickness of the effective cover, which acts as a thermal blanket; therefore, the thermal history of an exhumed footwall may record the original (post-emplacement) extent of a subsequently eroded thrust sheet (e.g., O'Hara et al., 1990). The areal extent of a thermal anomaly induced by excess cover constrains the magnitude of thrusting by showing the original (pre-erosion) extent and thickness of the thrust sheet over the footwall. As an example, the Jones Valley fault in the southern Appalachian thrust belt in Alabama, USA, is exposed along a northwest-directed, large-scale frontal ramp (Fig. 1); the leading part of the Jones Valley thrust sheet, including the leading hanging-wall cutoffs, has been eroded. Previously published (Winston, 1990a) vitrinite reflectance data document a distinct thermal anomaly northwest of the trace of the Jones Valley fault; a map of coal rank, using volatile matter and vitrinite reflectance, confirms the extent of the anomaly (Fig. 2)[1] (Pashin et al., 2004, 2008). The location of the thermal anomaly corresponds to that of the possible original leading part of the Jones Valley thrust sheet, which has been eroded. The purpose of this research is to quantify the possible original extent and geometry of the thrust sheet in the context of the location and magnitude of the thermal anomaly in the eroded footwall.

GEOLOGIC SETTING OF THE THERMAL ANOMALY

The previously documented thermal anomaly has an elongate, oval shape parallel to regional structural strike along the southeastern edge of the Black Warrior foreland basin at the leading edge of the Appalachian thrust belt (Figs. 1 and 2). The southeast boundary of the anomaly is along the Blue Creek anticline-syncline pair, relatively low-amplitude structures northwest

*Present address: BP America Inc., 200 Westlake Park Boulevard, Houston, Texas 77079-2663, USA

[1]If you are viewing the PDF of this paper, or if you are reading this offline, please visit http://dx.doi.org/10.1130/GES00168.S1 or the full-text article on www.gsajournals.org to access the layered PDF of Figure 2.

Geosphere; October 2008; v. 4; no. 5; p. 814–828; doi: 10.1130/GES00168.1; 8 figures; 2 tables.

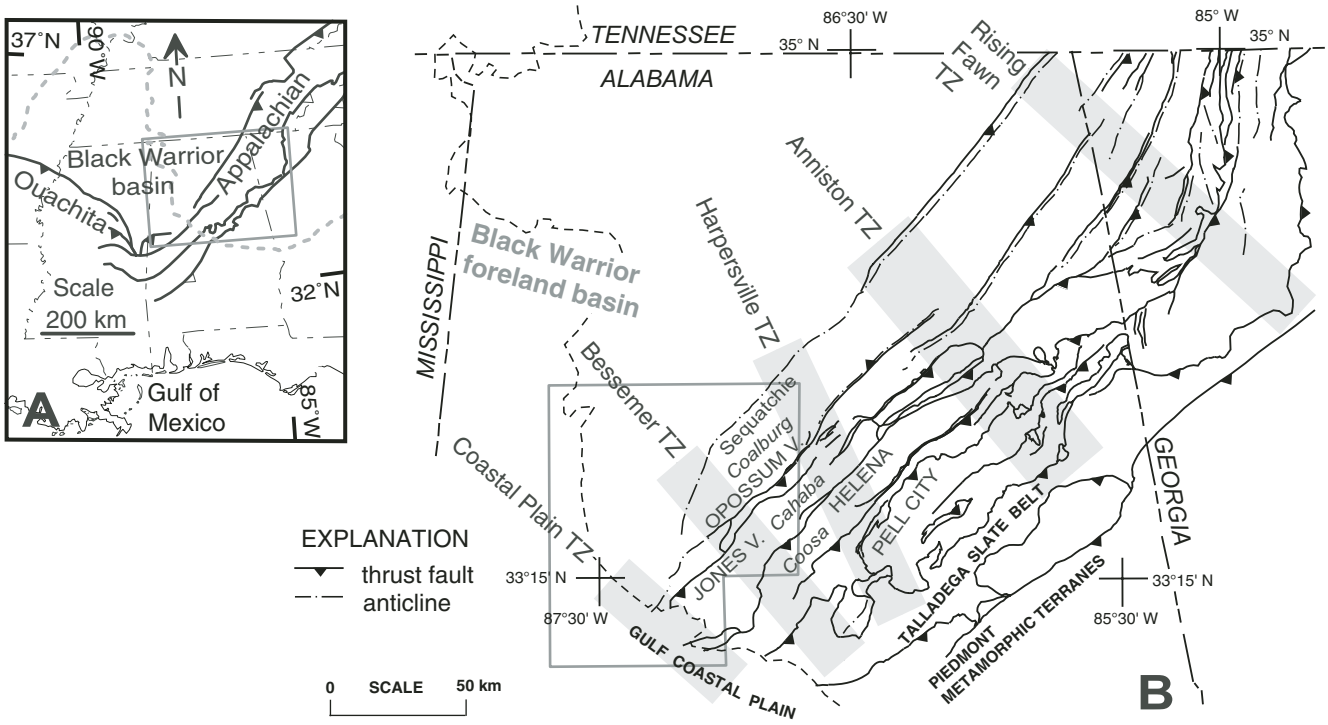

Figure 1. (A) Regional map of Appalachian-Ouachita thrust belt and Black Warrior foreland basin. Dashed gray line shows limit of Gulf Coastal Plain. Gray rectangle shows area of B. (B) Outline map of structural geology of Appalachian thrust belt in Alabama and Georgia. Names of regional syncline and synclinoria are shown in italics. Gray outline shows area of Figure 2. TZ—transverse zone; V—valley.

of the trace of the Jones Valley thrust fault (Fig. 2). The anomaly ends northeastward along strike at the Bessemer transverse zone, an alignment of cross-strike links (lateral ramps and displacement-transfer zones) across the Appalachian thrust belt (Figs. 1 and 2). At the Bessemer transverse zone, the Opossum Valley thrust sheet ends southwestward along strike in the footwall of the Jones Valley fault, and displacement is transferred via a dextral lateral ramp to the Jones Valley fault. The southwest end of the anomaly is across strike northwest of a sinistral curve in the Jones Valley fault, indicating a sinistral lateral ramp (Fig. 2).

The Pennsylvanian Pottsville Formation forms all of the present outcrop area in the footwall and more distal foreland of the Jones Valley fault, including the area of the vitrinite reflectance anomaly. The Pottsville Formation includes two distinct parts (Fig. 3). The lower Pottsville is characterized by relatively quartzose massive sandstones and includes thin shale intervals and some coal beds. The upper Pottsville has a classic "coal measures" stratigraphy, dominated by mudstones and including numerous coal beds and some sandstone (Fig. 3) (Pashin, 2004, 2005). These are the commercial mineable coals of the Warrior coal field and are also the resource for coalbed methane production. Exposed and subsurface coal beds provide for an array of samples for vitrinite reflectance analyses to document the extent and magnitude of the thermal anomaly.

DOCUMENTATION OF THE THERMAL ANOMALY

Data

This study combines previously published vitrinite reflectance data (Table 1) (Winston, 1990a) with new data (Table 2). The previously published data (Table 1) are measurements of mean maximum vitrinite reflectance (%R_{max}), whereas the newly collected data (Table 2) are measurements of mean random vitrinite reflectance (%R_o). A standard conversion of %R_{max} = 1.06 %R_o (Hower, 1978) was applied (Table 1) for preparation of the contour map of reflectance values in Figure 2.

Coal samples have been collected from outcrops, underground mines, surface mines, core holes, coalbed methane wells, and petroleum exploration wells. The samples span the stratigraphic range of coal beds from the Brookwood coal group down into the lower Pottsville (Fig. 3). Localities for collection of new samples for this research were spaced around the location of the previously recognized thermal anomaly, as well as more distant from the anomaly to confirm background values.

Geothermal Gradient

Assuming a steady state, where the upward heat flow is constant, the geothermal gradient is given by $\lambda = q/k$, where q is heat flow and k is the thermal conductivity of the rock. The geothermal gradient varies from one lithology to another, especially in coal-bearing shale-rich successions (e.g., Fig. 3), because the thermal conductivities of shale and coal are much less than those of limestone and sandstone (Blackwell and Steele, 1989). As a result, a succession of shale and coal acts as a thermal blanket and, locally at least, increases the geothermal gradient (Cercone et al., 1996).

In several core holes and wells, coal samples from multiple horizons were analyzed. From these vertical successions of data, a geothermal gradient was calculated by converting %R to temperature (T), using the time-independent equation, T(°C) = [ln(%R) + 1.26]/0.00811, from Barker and Goldstein (1990). Calculations from different boreholes indicate geothermal gradients between ~65 °C/km and ~35 °C/km (Fig. 4).

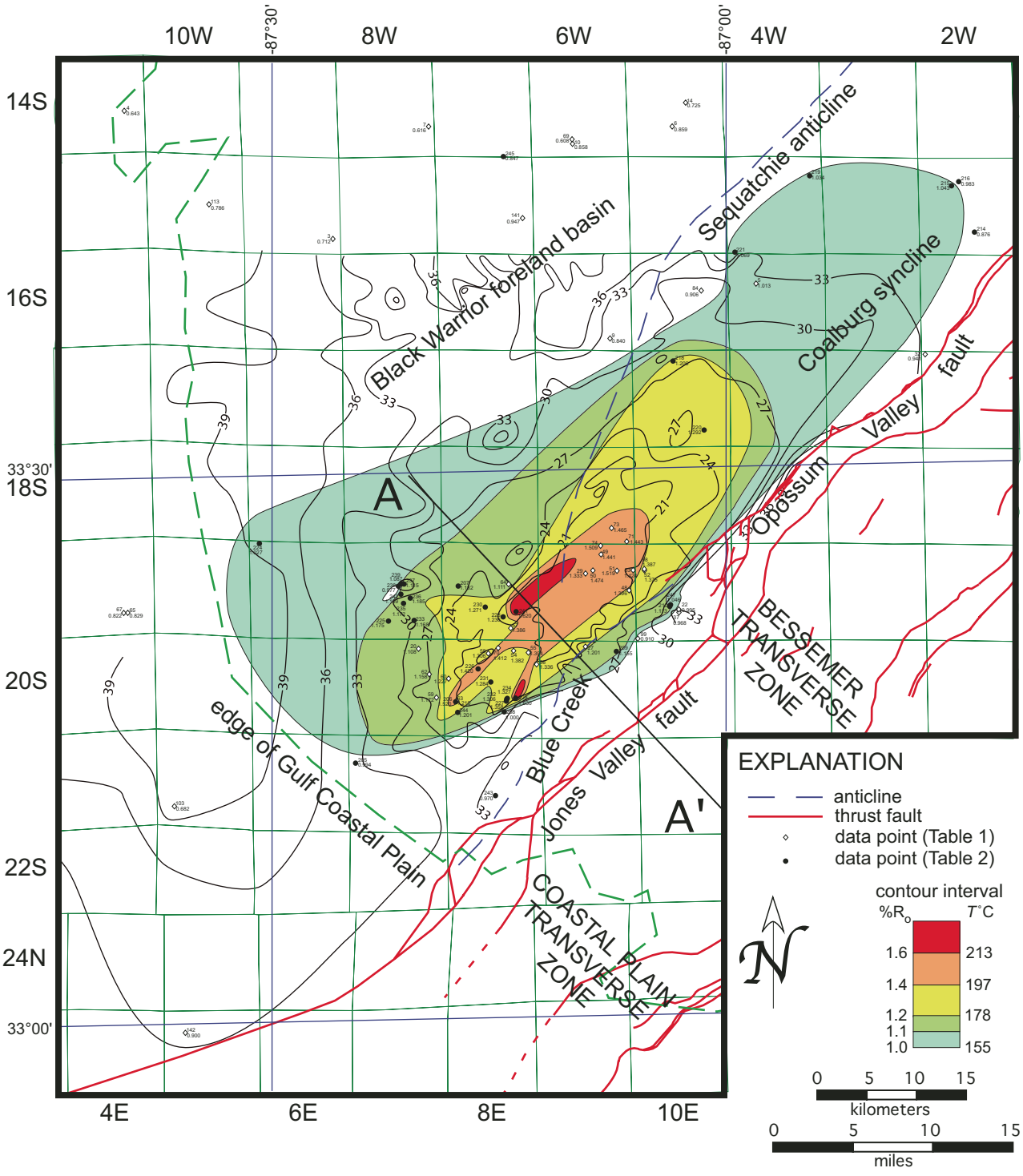

Figure 2 (see footnote 1). Map of thermal data in relation to geologic structures. See text for discussion of relation of the thermal anomaly (%R_o >1.2) to the Jones Valley thrust fault, as well as to the Bessemer and Coastal Plain transverse zones. Location of map shown in Figure 1B. Map shows line of cross-section A–A' (Fig. 8). The map is in five layers, which may be viewed in any combination. LAYER: Structure Outline—structural outline map of the northwestern part of the Appalachian thrust belt in central Alabama (modified from Osborne et al., 1988, and Szabo et al., 1988) and locations of data points. LAYER: R_o Contour Map—contour lines show distribution of %R_o (vitrinite reflectance) from published %R_{max} data (Table 1; from Winston, 1990a) and measured %R_o (Table 2). Temperature conversion of %R_o values uses the equation T(°C) = [ln(%R) + 1.26]/0.00811 (from Barker and Goldstein, 1990). LAYER: Township Grid—land survey grid for location. LAYER: Samples & Data—map numbers for sample locations and R_o data from Tables 1 and 2 (requires enlargement to make numerals readable). LAYER: Volatile Matter—contour map of percent volatile matter (dry mineral-matter-free) in coals (from Pashin et al., 2004).

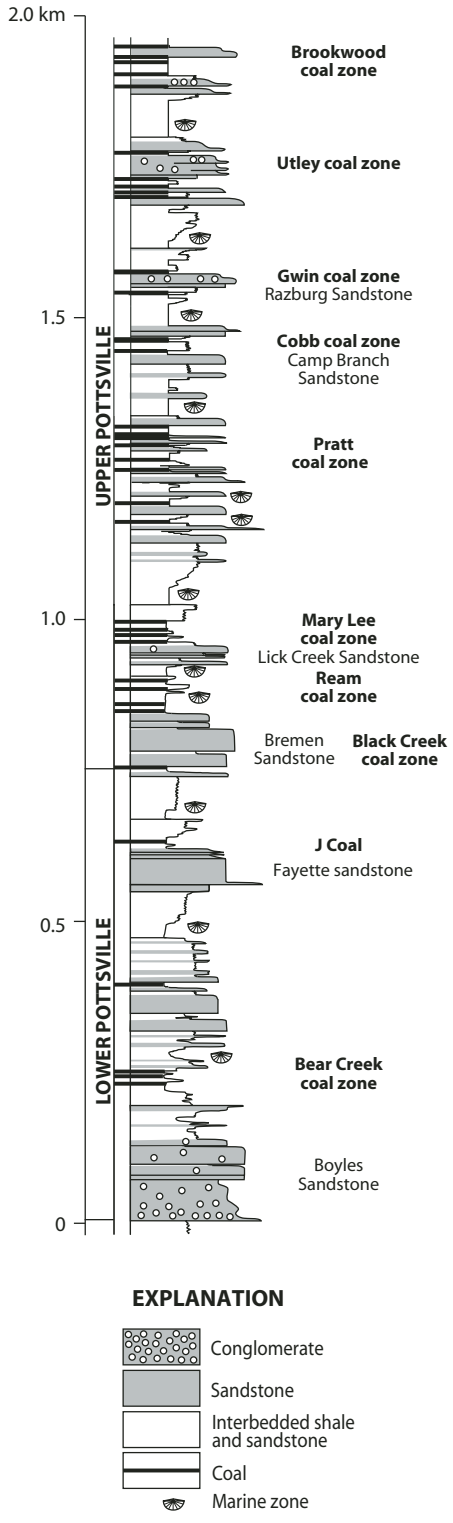

Figure 3. Stratigraphic column, showing lithologic succession and named coal zones (groups) in the Pennsylvanian Pottsville Formation in the Black Warrior foreland basin adjacent to the frontal Appalachian thrust faults (from Pashin, 2005). Stratigraphic levels of samples for vitrinite reflectance (Tables 1 and 2) are identified by coal bed and coal group.

Vitrinite reflectance data for the Mary Lee coal (Fig. 3) show a consistent regional background with %R values of <1.0 (Winston, 1990a), indicating a maximum temperature of ~155 °C. Density logs show that shale in the coal-bearing succession is fully compacted, indicating a minimum thickness of sedimentary cover of ~3 km (Hines, 1988). A thickness of 3 km of sedimentary cover is consistent with %R = 1.0 for Mary Lee coal (Carroll et al., 1993) and an average geothermal gradient of 45 °C/km. The computed local geothermal gradient through the coal-bearing interval in two boreholes is 64 °C/km (Fig. 4). The gradient cannot be that great through the entire stratigraphic section within the thermal anomaly, however, because an average geothermal gradient of 64 °C/km through a 3-km-thick cover would yield background temperatures of >200 °C at the Mary Lee stratigraphic level, higher than documented thermal indicators. The geothermal gradient is steepened by low thermal conductivity in successions with relatively high proportions of shale and coal, and the measured 64 °C/km gradient apparently is a stratigraphically localized anomaly. A regional gradient of 45 °C/km is more appropriate here and is similar to measured gradients of 38–47 °C/km in the coal-bearing shale-dominated successions of the Appalachian basin in Pennsylvania (Cercone et al., 1996).

The applicability of an average geothermal gradient of 45 °C/km for this area can be tested for the stratigraphic section shown in Figure 3, by weighting the thermal conductivities of different lithologies with respect to thicknesses. Figure 3 indicates ~45% sandstone, >53% shale, and <2% coal over a total thickness of 2 km. Assuming thermal conductivities of 2.5, 1.0, and 0.2 W/mK for sandstone, shale, and bituminous coal, respectively (Singer and Tye, 1979; Blackwell and Steele, 1989), the mean thermal conductivity is 1.66 W/mK. This value is the same as that estimated by Cercone et al. (1996) for the stratigraphic column in the northern Appalachian basin. A geothermal gradient of 45 °C/km indicates a heat flow of 75 mW/m^2, which is a reasonable value for a continental orogenic site (Bott, 1982).

Normalizing the Data to the Depth of the Mary Lee Coal

To remove the thermal effects of different amounts of sedimentary burial at different stratigraphic levels, vitrinite data from stratigraphically higher and lower coals were normalized to the stratigraphic level of the Mary Lee coal by using the geothermal gradient in a particular bore hole or by using a gradient of 64 °C/km for the coal-bearing interval (Tables 1 and 2). The Mary Lee coal was selected for the norm because more data are from that level than any other, and because it is near the middle of the stratigraphic interval of data sources.

MAP DISTRIBUTION OF THE THERMAL ANOMALY

The data normalized to the Mary Lee level closely constrain a local thermal anomaly northwest of the eroded leading edge of the Jones Valley thrust sheet (Fig. 2). The oval anomaly is elongate parallel to northeasterly Appalachian structural strike, and it ends in both directions along strike. Steep gradients define both the northwest and southeast edges of the anomaly. The area of anomalously high coal rank is ~300 km^2 and has vitrinite reflectance values of 1.2–1.6 %R_o, a maximum of >0.6 %R_o above the regional background (Fig. 2) (Culbertson, 1964; Telle et al., 1987; Winston, 1990a, 1990b; Pashin and Hinkle, 1997).

DISCUSSION OF POSSIBLE CAUSES OF THE THERMAL ANOMALY

Various causes have been or can be suggested for the thermal anomaly. The oval-shaped geometry and areal extent of the anomaly impose significant constraints on the cause. The anomaly has a relatively small area and relatively steep gradients, especially at the southeast and northwest margins, giving a short-wavelength–high-amplitude (steep gradient) profile. Therefore, possible causes that yield a long-wavelength–low-amplitude (gentle gradient) profile are rendered unlikely. The thermal anomaly must be a result of locally higher temperature than the regional temperature (Winston, 1990b).

Possible causes of increased heat flow include plutonism at depth (e.g., Telle et al., 1987) and/or excess radioactivity in the underlying crust. Lack of a gravity or magnetic anomaly associated with the area of high-rank coal (Winston, 1990b), as well as a lack of other independent verification and a lack of known late Paleozoic plutons in the southern Appalachian thrust belt, casts doubt on the former interpretation. Excess radiogenic heat from the crust would produce a broad, long-wavelength–low-amplitude thermal anomaly, unlike the configuration of the documented anomaly. Although frictional heating along active faults may be important on a centimeter scale, it is not thought to be important on a kilometer scale during thrust emplacement (e.g., Bustin, 1983; O'Hara, 2004).

Advective heat transport associated with local uplift and rapid erosion provides another alternative heating mechanism. Rapid removal of ~3 km of overburden could produce substantial

TABLE 1. PUBLISHED VITRINITE REFLECTANCE DATA

Sample	Number on map (Fig. 2)	Source of sample (depth in core hole or well in feet)*	Coal group	Coal bed	R_{max}	Stratigraphic interval above or below Mary Lee coal (feet)*	R_{max} normalized to Mary Lee coal†	Equivalent R_o§
3	3	surface mine	Cobb	Lower? Cobb	0.699	948	0.755	0.712
4	4	surface	Pratt	Pratt	0.647	584	0.681	0.643
5	5	surface	Pratt	American	1.040	584	1.074	1.013
6	6	surface mine	Black Creek	Black Creek	0.933	–378	0.911	0.859
7	7	surface	Mary Lee	New Castle	0.653	0	0.653	0.616
9	9	surface	Pratt	American	0.856	584	0.890	0.840
10	10	surface	Mary Lee	Mary Lee	0.910	0	0.910	0.858
14	14	surface	Black Creek	Black Creek?	0.791	–378	0.769	0.725
20	20	mine	Mary Lee	Blue Creek	1.179	0	1.179	1.112
21		mine	Mary Lee	Mary Lee	1.170	0	1.170	1.104
22	22		Mary Lee	Jagger	1.055	0	1.055	0.995
27	27	mine	Mary Lee	Mary Lee	1.261	0	1.261	1.190
28		mine	Mary Lee	Blue Creek	1.285	0	1.285	1.212
29	29	core (1324.5)	Mary Lee	Blue Creek	1.512	0	1.512	1.426
30		core (1319.4)	Mary Lee	Mary Lee	1.505	0	1.505	1.420
31		core (1278.0)	Mary Lee	New Castle	1.541	0	1.541	1.454
38		core (142.0)	Gwin	Upper Gwin	1.301	1178	1.370	1.293
39		core (203.0)	Gwin	Thompson Mill?	1.179	1117	1.245	1.174
40		core (373.0)	Cobb	Upper Cobb	1.351	947	1.407	1.327
41		core (385.0)	Cobb	Lower Cobb	1.299	935	1.354	1.277
42		core (706.0)	Pratt	Pratt	1.411	614	1.447	1.365
43		core (790.0)	Pratt	American?	1.419	530	1.450	1.368
44		core (835.0)	Pratt	Lower American	1.369	485	1.397	1.318
45		core (895.0)	Pratt	Curry	1.306	425	1.331	1.256
46		core (940.0)	Pratt	Gillespy	1.374	380	1.396	1.317
32	32		J	Tidmore or Lower J	1.048	–867	0.997	0.941
37	37		Mary Lee	Blue Creek	1.026	0	1.026	0.968
48	48	mine	Mary Lee	Blue Creek	1.480	0	1.480	1.396
49	49	mine	Mary Lee	Blue Creek	1.527	0	1.527	1.441
50	50	mine	Mary Lee	Blue Creek	1.562	0	1.562	1.474
51	51	mine	Mary Lee	Blue Creek	1.610	0	1.610	1.519
52	52	mine	Mary Lee	Blue Creek	1.457	0	1.457	1.375
53	53	mine	Mary Lee	Blue Creek	1.509	0	1.509	1.424
54	54	mine	Mary Lee	Blue Creek	1.465	0	1.465	1.382
55	55	mine	Mary Lee	Blue Creek	1.478	0	1.478	1.394
56	56	mine	Mary Lee	Blue Creek	1.416	0	1.416	1.336
57	57	mine	Mary Lee	Blue Creek	1.469	0	1.469	1.386
58	58	mine	Mary Lee	Blue Creek	1.384	0	1.384	1.306
59	59	mine	Mary Lee	Blue Creek	1.242	0	1.242	1.172
60	60	mine	Mary Lee	Blue Creek	1.301	0	1.301	1.227
62	62	mine	Mary Lee	Blue Creek	1.227	0	1.227	1.158
63	63	mine	Mary Lee	Blue Creek	1.283	0	1.283	1.210
64	64	mine	Brookwood	Upper Clements	1.071	1823	1.178	1.111
65	65	well (1880–1940)	Mary Lee		0.861	0	0.861	0.812
66		well (2290–2350)	Black Creek		0.921	–410	0.897	0.846
67	67	well (1900–1940)	Mary Lee		0.824	0	0.824	0.777
68		well (2300–2310)	Black Creek		0.941	–400	0.918	0.866
69	69	mine	Mary Lee	New Castle	0.644	0	0.644	0.608
70	70	mine	Mary Lee	Blue Creek	1.497	0	1.497	1.412
71	71	mine	Mary Lee	Blue Creek	1.530	0	1.530	1.443
73	73	mine	Mary Lee	Blue Creek	1.553	0	1.553	1.465
74	74	mine	Mary Lee	Blue Creek	1.600	0	1.600	1.509
78	west of Fig. 2#	well (3070–3090)	Gwin?		0.936	1672	1.034	0.976
79		well (3510–3530)	Cobb?		1.016	1232	1.088	1.027
80		well (5120–5130)	Black Creek?		1.220	–378	1.198	1.130
84	84	core (170.5)	Black Creek		0.922	–258	0.907	0.856
85		core (191.6)	Black Creek		0.948	–280	0.932	0.879
86		core (198.4)	Black Creek		0.871	–286	0.854	0.806
88		core (207.8)	Black Creek		0.948	–296	0.931	0.878
89		core (236.8)	Black Creek		0.998	–325	0.979	0.924
90		core (239.6)	Black Creek		1.070	–328	1.051	0.991

(*continued*)

TABLE 1. PUBLISHED VITRINITE REFLECTANCE DATA (continued)

Sample	Number on map (Fig. 2)	Source of sample (depth in core hole or well in feet)*	Coal group	Coal bed	R_{max}	Stratigraphic interval above or below Mary Lee coal (feet)*	R_{max} normalized to Mary Lee coal†	Equivalent R_o§
91	84	core (239.9)	Black Creek		1.007	–328	0.988	0.932
92		core (623.0)	J		0.876			
93		core (513.0)	J	J?	0.937			
94		core (637.0)	J		0.887			
95		core (530.0)	J	K?	0.930			
96		core (638.0)	J		0.870			
97		core (290.0)	Black Creek		1.059	–378	1.037	0.978
98	98		Mary Lee	Blue Creek	1.470	0	1.470	1.387
99	99		J?		1.016	–867	0.965	0.910
103	103	well (2729)	Mary Lee		0.723	0	0.723	0.682
113	113	well (630–640)	Mary Lee		0.860	0	0.860	0.811
114		well (1800–1810)	J		0.875	–1170	0.806	0.761
141	141	mine	Mary Lee		1.004	0	1.004	0.947
142	142	well (1163.0)	Utley	Utley	0.717	2495	0.864	0.815
143		well (1651.0)	Gwin	Gwin	0.839	2007	0.957	0.903
144		well (1658.0)	Gwin	Thompson Mill	0.898	2000	1.015	0.958
145		well (2604.0)	Pratt	Fire Clay (Pratt)	0.896	1054	0.958	0.904
146		well (3658.0)	Mary Lee	Mary Lee	0.953	0	0.953	0.899
147		well (3659.7)	Mary Lee	Upper Blue Creek	0.979	0	0.979	0.924

Note: Data from Winston (1990a).

*The original records of wells and core holes have measurements in feet; for efficiency in relating tabulated data to the original records, the tables retain the original measurements in feet (1 ft = 0.3048 m).

†Using geothermal gradient in a particular borehole or average geothermal gradient for the coal-bearing interval of 64 °C/km = 0.0000587 R_o/ft.

§Using the relationship $\%R_{max} = 1.06\ \%R_o$.

#Location is 53.4 km due west of the southwest corner of Figure 2.

heating in ~500 k.y. (Turcotte and Schubert, 2002); however, the wavelength and amplitude of the documented anomaly require a local steep-sided uplift that is precluded by the outcrop and subsurface geology. A regional isostatic uplift would have a long wavelength relative to amplitude. The estimated heat flow (~75 mW/m^2) is not anomalous for this region, suggesting that local anomalous heat flow is not the cause of the anomaly.

Hydrothermal fluid flow also has been suggested as a cause of the anomaly (e.g., Winston, 1990a), involving either orogenic fluids derived from the Appalachian orogen on the southeast (e.g., Goldhaber et al., 2003) or circulation of hot meteoric water. Calcite-filled fractures (joints and cleats) in the Pottsville Formation indicate that fractures did serve as conduits for fluid flow in the basin (Pitman et al., 2003). Oxygen isotope analyses of the calcite, however, indicate that this fluid flow is consistent with influx of low-temperature (30–50 °C) meteoric water late in the history of the basin. This water would have been too cool to cause the observed anomaly in the coals of ~50 °C above background (~155 °C) at the depth of the Mary Lee coal. The lack of higher temperature hydrothermal mineralization in the coal cleats that formed during maturation (Pitman et al., 2003) argues against a hydrothermal origin for coal maturation. Orogenic fluids derived from the southeast would be unlikely to produce the observed oval-shaped anomaly, which is separated from the frontal large-scale thrust fault and isolated in the foreland; instead, such an anomaly would be expected to extend into the foreland directly from the structural front, contrary to the observed pattern. In the absence of shallow-level igneous plutons beneath the anomaly, convective circulation of hot groundwater is also an unlikely source of the anomaly.

Localized excess thickness of sedimentary cover is a possible cause of a thermal anomaly. The observed area of anomalous coal rank, however, cannot be explained by a locally greater depositional thickness of sedimentary cover because the contours of %R are not affected by the Blue Creek anticline (Fig. 2), indicating late syntectonic to posttectonic coalification (Winston, 1990a; Pashin et al., 1999). Furthermore, the local magnitude and abrupt boundaries of the anomaly are not compatible with reasonable gradients of depositional thickness in a foreland basin, such as the setting of Pottsville deposition (Thomas, 1988; Pashin, 2004).

We propose, instead, that the thermal anomaly is primarily the result of local excess tectonic cover caused by emplacement of a thrust sheet (O'Hara et al., 2006). The anomaly is inferred to be in the footwall of the now-eroded thrust sheet, the eroded leading trace of which is the Jones Valley fault southeast of the anomaly (Fig. 2). Both along-strike ends of the anomaly are aligned with lateral ramps, a dextral lateral ramp on the northeast and a sinistral lateral ramp on the southwest. A three-dimensional thermal model is needed to test whether a thrust sheet of the possible dimensions of the Jones Valley thrust sheet will account for the documented thermal environment.

DESIGN OF A THREE-DIMENSIONAL COOLING MODEL

That thin-skinned thrust sheets are commonly bounded by both frontal and trailing ramps has been long recognized (e.g., Rich, 1934; Boyer and Elliott, 1982). Similarly, along-strike terminations of thrust sheets at lateral ramps, transverse faults, displacement-transfer zones, and displacement gradients are widely recognized (Boyer and Elliott, 1982; Laubscher, 1985; Price, 1988; Thomas, 1990; Thomas and Bayona, 2002). In a model thrust sheet (Fig. 5), after thrust emplacement, cooling is inferred to occur laterally across a leading hanging-wall frontal ramp, two hanging-wall lateral ramps, and a trailing hanging-wall fault-bend fold over a footwall frontal ramp, as well as downward by heating of the footwall. This requires three-dimensional modeling to better understand the thermal history of both the hanging wall and footwall.

Three-dimensional cooling of an instantaneously emplaced thrust sheet with horizontal dimensions of 10 × 30 km and a thickness of 3 km is used to model the coal-rank anomaly mapped in Figure 2. These dimensions were selected to represent the mapped extent of the thermal anomaly and the maximum excess

TABLE 2. MEASURED VITRINITE REFLECTANCE

Sample	Number on map (Fig. 2)	Source of sample (depth in core hole or well in feet)*	Geological Survey of Alabama reference number	Coal group	Coal bed	Latitude (°N)	Longitude (°W)	R_o	Stratigraphic interval above or below Mary Lee coal (feet)*	R_o normalized to Mary Lee coal†
5b	205	mine		Brookwood	Brookwood	33.22768	87.41485	0.924451	1823	1.031523
5c		mine		Brookwood	Carter	33.22768	87.41485	0.848046	1823	0.955118
6	206	mine		Mary Lee	Blue Creek	33.28212	87.30598	1.519631	0	1.519631
7	207	outcrop		Utley		33.38705	87.30142	1.080739	1723	1.181938
8	208	outcrop		Brookwood		33.27233	87.25365	0.892646	1823	0.999718
9j	209	surface mine		Mary Lee	Jagger	33.32570	87.13153	1.177092	0	1.177092
9lbc		surface mine		Mary Lee	Lower Blue Creek	33.32570	87.13153	1.132074	0	1.132074
10l	210	outcrop		Curry?	Clemens	33.36573	87.07308	1.097354	353	1.118087
10u		outcrop		Curry?	Clemens	33.36573	87.07308	1.087222	353	1.107955
14	214	outcrop		Mary Lee		33.70027	86.73597	0.875537	0	0.875537
15c	215	outcrop		Mary Lee		33.74265	86.75992	1.022315	0	1.022315
15s		outcrop		Mary Lee		33.74265	86.75992	1.062928	0	1.062928
16l	216	outcrop		Mary Lee		33.74630	86.75203	0.983487	0	0.983487
17	217	core	AL-CU-TP1-2.0	Black Creek	Black Creek	33.89367	87.03267	0.940046	–378	0.917845
18a	218	core	AL-JE-BCCFT-1.0	Pratt	Nickel Plate	33.58823	87.06528	1.188361	584	1.222662
18b		core	AL-JE-BCCFT-2.0	Curry	Curry	33.58823	87.06528	1.168476	353	1.189209
19	219	core	AL-JE-MRM-1.0	Black Creek	Jefferson	33.75413	86.91369	1.056267	–378	1.034066
20	220	core (215.3)	AL-JE-SCCH-0215.3	Gwin	Gwin	33.52520	87.03282	1.215444	1295	1.291505
21	221	core	AL-JE-TPLM-1.0	Mary Lee	Mary Lee	33.68605	86.99623	1.068766	0	1.068766
22	222	core	AL-MA-MB2-1.0	Black Creek	Black Creek	34.07937	87.74402	0.917525	–378	0.895324
24	224	core (1690.2)	AL-TU-EPBC-1690.2	Mary Lee		33.42799	87.51589	1.027452	0	1.027452
25	225	core	AL-TU-JWR41-2.0	Mary Lee	Blue Creek	33.35614	87.37737	1.175055	0	1.175055
26a	226	core (1400.0)	AL-TU-JWR626-1400.0	Pratt	#1	33.31167	87.28118	1.317632	548	1.349818
26b		core (1947.5)	AL-TU-JWR626-1947.5	Mary Lee	New Castle	33.31167	87.28118	1.488920	0	1.488920
27	227	core (2105.0)	AL-TU-JWR628-2105.0	Mary Lee	Jagger	33.28205	87.25115	1.357739	0	1.357739
28	228	core (1695.1)	AL-TU-JWR629-1695.1	Mary Lee	New Castle	33.35853	87.25335	1.235682	0	1.235682
29	229	core (636.7)	AL-TU-JWR630-0636.7	Gwin	Gwin	33.28477	87.24127	1.554010	1295	1.630071
30	230	core (986.9)	AL-TU-JWR632-0986.9	Pratt	#1	33.36762	87.27253	1.236371	584	1.270672
31a	231	core (613.7)	AL-TU-JWR633-0613.7	Gwin	Gwin	33.29960	87.26770	1.229921	1427	1.313735
31b		core (1411.5)	AL-TU-JWR633-1411.5	Pratt	#1	33.29960	87.26770	1.214263	629	1.251207
31c		core (2041.0)	AL-TU-JWR633-2041.0	Mary Lee	Jagger	33.29960	87.26770	1.287485	0	1.287485
32a	232	core (937.3)	AL-TU-JWR638-0937.3	Cobb	Cobb	33.28377	87.25077	1.160606	1167	1.229149
32b		core (1406.8)	AL-TU-JWR638-1406.8	Pratt	#2	33.28377	87.25077	1.311426	697	1.352364
32c		core (2104.0)	AL-TU-JWR638-2104.0	Mary Lee	Jagger	33.28377	87.25077	1.337272	0	1.337272
33	233	core (2346.2)	AL-TU-JWR639-2346.2	Black Creek	Black Creek	33.35645	87.34957	1.190470	–378	1.168269
34a	234	core (688.8)	AL-TU-JWR640-0688.8	Gwin	Gwin	33.28455	87.25008	1.205133	1467	1.291296
34b		core (1402.5)	AL-TU-JWR640-1402.5	Pratt	#4	33.28455	87.25008	1.231743	754	1.276028
34c		core (2156.4)	AL-TU-JWR640-2156.4	Mary Lee	Jagger	33.28455	87.25008	1.351230	0	1.351230
34d		core (2577.8)	AL-TU-JWR640-2577.8	Black Creek	Black Creek	33.28455	87.25008	1.414711	–422	1.389925
35	235	core (1724.5)	AL-TU-JWR650-1724.5	Mary Lee	New Castle	33.37202	87.36083	1.171868	0	1.171868
36a	236	core (1141.6)	AL-TU-JWR652-1141.6	Pratt		33.37673	87.35347	1.136152	570	1.169630
36b		core (1711.7)	AL-TU-JWR652-1711.7	Mary Lee	New Castle	33.37673	87.35347	1.221648	0	1.221648
36c		core (2190.0)	AL-TU-JWR652-2190.0	Black Creek	Black Creek	33.37673	87.35347	1.191828	–478	1.163753
37	237	core (2193.2)	AL-TU-JWR653-2193.2	Black Creek	Black Creek	33.38955	87.35997	1.142957	–478	1.114882

(*continued*)

TABLE 2. MEASURED VITRINITE REFLECTANCE (continued)

Sample	Number on map (Fig. 2)	Source of sample (depth in core hole or well in feet)*	Geological Survey of Alabama reference number	Coal group	Coal bed	Latitude (°N)	Longitude (°W)	R_o	Stratigraphic interval above or below Mary Lee coal (feet)*	R_o normalized to Mary Lee coal†
38a	238	core (227.7)	AL-TU-JWR654-0227.7	Gwin	Gwin	33.38763	87.36613	0.826408	1509	0.915038
38b		core (1737.0)	AL-TU-JWR654-1737.0	Mary Lee	New Castle	33.38763	87.36613	1.039186	0	1.039186
39	239	core (1205.3)	AL-TU-JWR655-1205.3	Pratt		33.38995	87.36285	1.053030	584	1.087331
41	241	core (2118.9)	AL-TU-JWR656-2118.9	Black Creek	Black Creek	33.36310	87.23923	1.642459	–378	1.620258
42a	242	core (1208.3)	AL-TU-JWR657-1208.3	Pratt		33.38035	87.36352	1.037710	558	1.070484
42b		core (1765.9)	AL-TU-JWR657-1765.9	Mary Lee	New Castle	33.38035	87.36352	1.109286	0	1.109286
43	243	core	AL-TU-MBR1-2.0	Mary Lee?		33.19650	87.26435	0.969860	0	0.969860
44	244	core	AL-TU-TRPM-3.0	Brookwood	Brookwood	33.27250	87.30385	1.093827	1823	1.200900
45	245	core	AL-WA-HV2-1.0	Mary Lee	Mary Lee	33.77603	87.24593	0.847063	0	0.847063
46	246	core	AL-WA-NV-1.0	Black Creek	Black Creek	33.99678	87.52083	0.809320	–378	0.787119
47a	247	core (350.0)	AL-JE-BCB1-350	Mary Lee	New Castle	33.36730	87.07220	0.878534	0	0.878534
47b		core (422.0)	AL-JE-BCB1-422	Mary Lee	New Castle	33.36730	87.07220	1.100779	0	1.100779
47c		core (550.0)	AL-JE-BCB1-550	Mary Lee	Jagger	33.36730	87.07220	0.863558	0	0.863558
47d		core (855.0)	AL-JE-BCB1-855	Black Creek		33.36730	87.07220	1.083371	–305	1.065457
47e		core (970.0)	AL-JE-BCB1-970	Black Creek		33.36730	87.07220	1.032762	–420	1.008094
47f		core (1417.0)	AL-JE-BCB1-1417	J?		33.36730	87.07220	1.141255	–867	1.090333
47h		core (2115.0)	AL-JE-BCB1-2115	upper Boyles		33.36730	87.07220	1.167737	–1565	1.075818
47i		core (2740.0)	AL-JE-BCB1-2740	lower Boyles		33.36730	87.07220	1.418934	–2190	1.290306

*The original records of wells and core holes have measurements in feet; for efficiency in relating tabulated data to the original records, the tables retain the original measurements in feet (1 ft = 0.3048 m).
†Using geothermal gradient in a particular borehole or average geothermal gradient for the coal-bearing interval of 64 °C/km = 0.0000587 R_o/ft.

temperature (~50 °C, Fig. 2) above the background level in the footwall within a reasonable time frame. A thrust sheet 3 km thick produces temperatures in the model that correspond to those indicated by vitrinite reflectance data (Fig. 2), and the 3 km thickness is consistent with stratigraphic thickness in thrust sheets regionally (Thomas and Bayona, 2005). In contrast, models using thrust sheets 5 km and 1 km thick produce temperatures that are greater and lesser, respectively, than those indicated by the vitrinite reflectance data. The oval heating pattern in the footwall (Fig. 2) is interpreted to represent the thermal imprint of the now-eroded thrust sheet. The sides of the thrust sheet are kept at constant ambient temperature ($T = T_o$), and the temperature with depth in the footwall is given by $T = T_b + \lambda(z - c)$, where T_b is temperature at the top of the footwall, λ is geothermal gradient, z is total depth, and c is thrust-sheet thickness. The 3D thermal diffusion equation to compute the temperature distribution, $T(x,y,z,t)$, is:

$$\nabla^2 T = \frac{\partial^2 T}{\partial x^2} + \frac{\partial^2 T}{\partial y^2} + \frac{\partial^2 T}{\partial z^2} = \frac{1}{\kappa}\frac{\partial T}{\partial t} ,$$

in the domain:

$$[0 \le x \le a; 0 \le y \le b; 0 \le z \le (1+f)c] , \qquad (1)$$

where T is temperature, x and y are orthogonal horizontal coordinates, z is depth (vertical direction and positive downward), κ is thermal diffusivity, t is time, a and b are the orthogonal horizontal dimensions of the thrust sheet, c is the thickness of the thrust sheet, and $(1+f)$ is the ratio of thickness in the footwall underlying the thrust sheet to that of the thrust sheet. The boundary conditions are given by equations 1b and 1c, and the initial condition is given by equation 1d (Appendix). The solution to this equation under these conditions is presented in the Appendix.

RESULTS OF THE THERMAL MODEL

The thermal model can be represented graphically for three-dimensional cooling at the center of a thrust sheet with dimensions of 3 × 10 × 30 km. Dimensionless depth is plotted against dimensionless temperature for different dimensionless times (Fig. 6). For both very rapid (e.g., Oxburgh and Turcotte, 1974) and geologically reasonable thrust velocities (1–10 cm/yr; Karabinos and Ketcham, 1988), the footwall undergoes heating (i.e., prograde metamorphism) because of downward heat flux across the thrust fault as the geotherm is reestablished. In the three-dimensional model (Fig. 6), the temperature reaches a steady state at ~2 m.y., and the geotherm never is fully reestablished, because

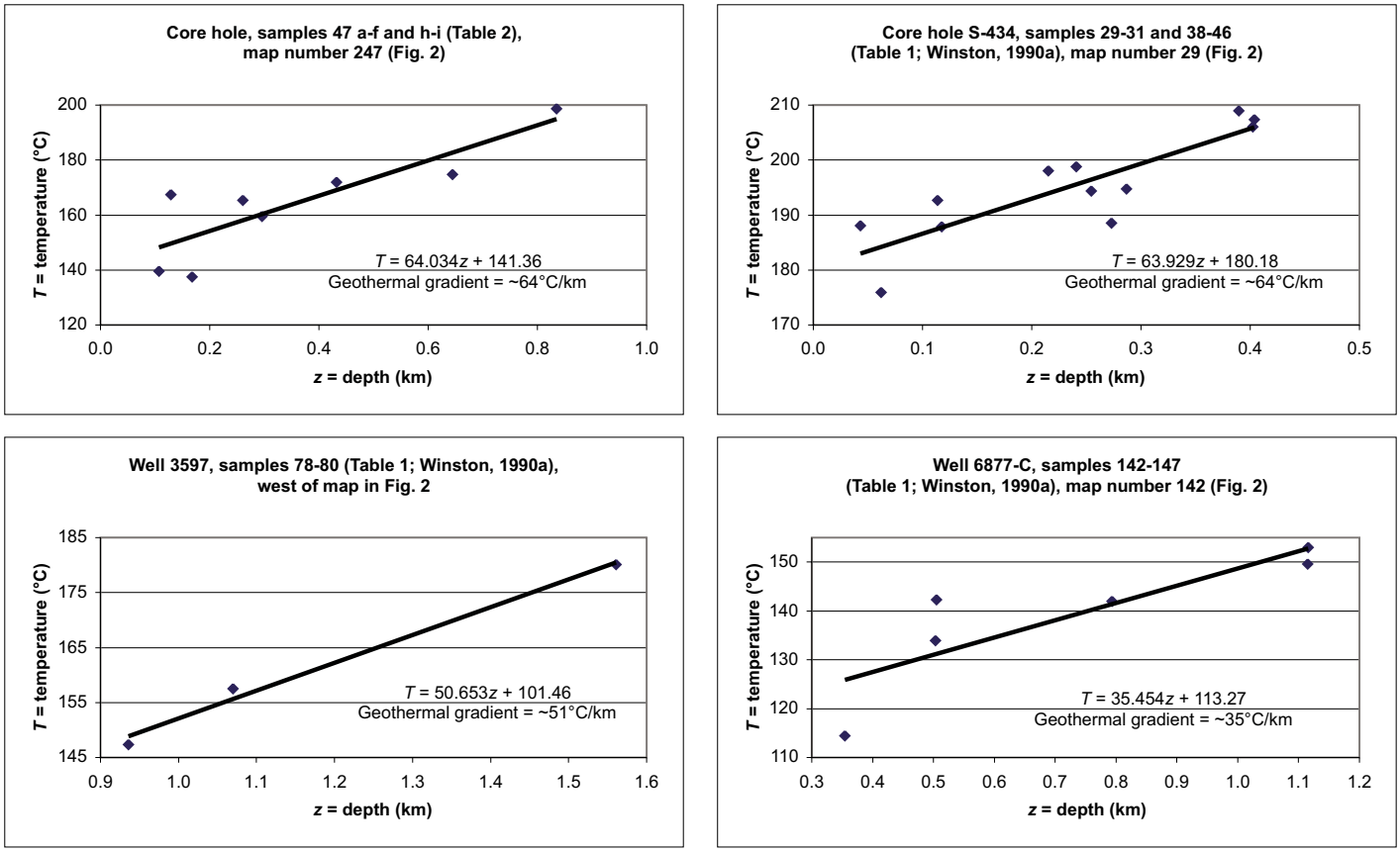

Figure 4. Computation of geothermal gradients from vertical successions of samples from each of four boreholes (data listed in Tables 1 and 2). Temperature conversion of $\%R_o$ values based on the equation $T(°C) = [\ln(\%R) + 1.26]/0.00811$ (Barker and Goldstein, 1990). Note that (1) for core hole S-434, the reported samples (Winston, 1990a) were not numbered consecutively (Table 1), and the omitted numbers were used for samples from other locations; (2) for the core hole at map number 247, data from repeated runs of sample 47g have too much scatter to be useful.

of lateral cooling of the thrust sheet. For earlier times, however, the results of one-dimensional and three-dimensional models are very similar (Fig. 6) (e.g., Furlong and Edman, 1984).

At the base of the thrust sheet in the model (Fig. 6), the dimensionless depth is 3 km/3 km = 1.0, and at the depth of the Mary Lee coal (3 km beneath the thrust fault) it is = 2.0. The dimensionless time τ (= $\kappa t/c^2$) at 1 m.y. is 3.5, where $\kappa = 10^{-6}$ m^2/s, $t = 3.15 \times 10^{13}$ s, and c = 3000 m. From Figure 6, these values (z/c = 2.0 and τ = 3.5) give a dimensionless temperature (scaling factor) of 1.3. The temperature at a depth of 3 km below the thrust fault at 1 m.y. is then [20 °C + (45 °C/km × 3 km)] × 1.3 = 202 °C. This temperature is close to the maximum attainable as the temperature reaches a steady state ~2 m.y. after thrusting.

Figure 7 shows the temperature contours at a depth of 3 km in the footwall for various times after emplacement of the thrust sheet. An elongated oval pattern develops after 100 k.y. (Fig. 7D) and intensifies up to 1 m.y. (Fig. 7F). Vertical cooling of the hanging wall and heating of the footwall, in combination with lateral cooling across the bounding ramps of the hanging wall, imprint an oval pattern of heating in the footwall. The maximum temperature obtained is ~200 °C (Fig. 7). Using the time-independent conversion of Barker and Goldstein (1990), this temperature is in good agreement with a $\%R_o$ value of 1.6, which corresponds to 213 °C. Using the kinetics-based software (EasyR%; Sweeney and Burnham, 1990) and a mean heating rate corresponding to ~200 °C over 500 k.y., a similar value for $\%R_o$ is calculated to be 1.55. Therefore, both a time-independent conversion and a time-dependent conversion of the observed $\%R_o$ values yield a similar temperature of ~200 °C. This temperature is close to the maximum obtainable using a three-dimensional cooling model at this depth (Fig. 6). The similarity between the observed vitrinite reflectance pattern (Fig. 2) and predicted isotherms (Fig. 7), in both shape and magnitude, suggests that the anomaly was caused by heating of the footwall by a now-eroded thrust sheet, which in addition to heating the underlying rocks, also cooled laterally. In this respect, the thermal anomaly is analogous to the burn pattern produced on a silk shirt by an overly hot clothes iron. For reasonable erosion rates (e.g., 1 mm/yr), a 3-km-thick thrust sheet would not be removed by erosion before heating of the footwall occurs (500 k.y.; Fig. 7E). Imbrication of the thrust sheet may have contributed to the thermal anomaly, and the thermal diffusivity may have been anisotropic, but for simplicity, these possibilities were not considered here.

A challenge to the applicability of the model is that the southeast margin of the thermal anomaly is along the Blue Creek anticline ~8 km northwest of the present trace of the Jones Valley fault at a frontal ramp (Fig. 2). The footwall immediately northwest of the present map trace of the Jones Valley fault shows background-level vitrinite reflectance. The geometry of the frontal ramp must accommodate that temperature distribution.

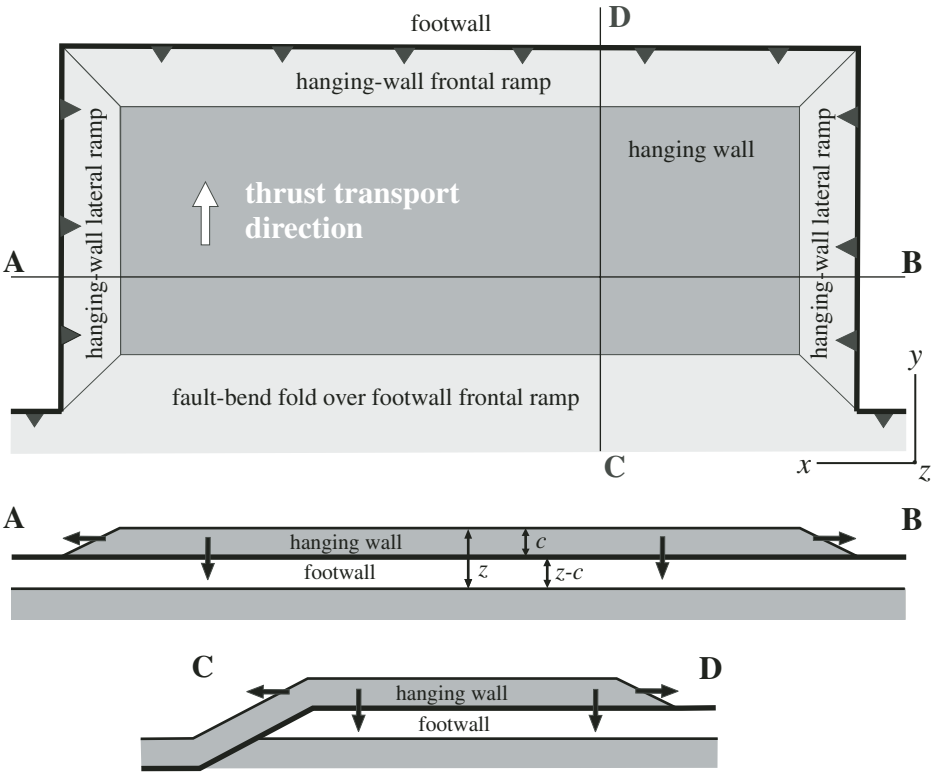

Figure 5. Generalized plan view and cross sections of a model thrust sheet bounded by a leading hanging-wall frontal ramp, two hanging-wall lateral ramps, and a trailing hanging-wall fault-bend fold over a footwall frontal ramp. Cross-section A–B (parallel to strike) illustrates hanging-wall lateral ramps; and cross-section C–D (perpendicular to strike) illustrates a leading hanging-wall frontal ramp and a trailing hanging-wall fault-bend fold over a footwall frontal ramp (modified after Thomas, 1990). Black arrows indicate directions of heat flow. Orientations of spatial dimensions *x*, *y*, and *z* are indicated. Boundary conditions are given in equations 1b and 1c (Appendix).

RELATIONSHIP OF THERMAL MODEL TO STRUCTURAL GEOLOGY

Northwest Edge of the Thermal Anomaly; Leading Edge of the Jones Valley Thrust Sheet

A balanced and restored structural cross section (Fig. 8) is consistent with the emplacement of a 3-km-thick thrust sheet 18 km northwestward onto the foreland, corresponding to the location and magnitude of the thermal anomaly. The now-eroded leading part of the thrust sheet is reconstructed to cover the area of the thermal anomaly (Fig. 8B). The palinspastic reconstruction (Fig. 8C) uses line-length balancing of the regional stiff layer (massive carbonates of the Upper Cambrian–Lower Ordovician Knox Group) and area balancing of the regional weak layer that hosts the Appalachian décollement (shale-dominated succession of Middle Cambrian–lower Upper Cambrian Conasauga Formation). The restored cross section is consistent with similarly restored cross sections along strike (Thomas and Bayona, 2005). The stratigraphic composition and thickness of the eroded thrust sheet are modeled from regional stratigraphy. The magnitude of the thermal anomaly indicates a total cover thickness above the Mary Lee coal group of ~6 km. This is modeled in the cross section as ~3 km of sedimentary cover in the footwall, indicated by the background coal rank outside the anomaly of <1.0%R_o (Fig. 2) and a 3-km-thick tectonic cover corresponding to the Jones Valley thrust sheet (Fig. 8). The structural cross section (Fig. 8B) shows an interpretation of the thickness and extent of the eroded part of the Jones Valley thrust sheet; the projection of an inferred synthrusting erosion surface limits the thrust-sheet thickness to 3 km, conforming to a total 6-km-thick cover necessary to account for the magnitude of the thermal anomaly. The palinspastically restored cross section (Fig. 8C) shows the relation of the stratigraphy in the now-eroded thrust sheet to that in the presently preserved footwall.

The northwest edge of the thermal anomaly is interpreted to mark the location of the hanging-wall frontal-ramp cutoff along the leading limb of a fault-bend (ramp) anticline at the leading edge of the Jones Valley thrust sheet. The northwestern gradient of the thermal anomaly corresponds to the northwestward thinning of the thrust sheet at the hanging-wall frontal ramp (Fig. 8). The highest temperature values in the thermal anomaly correspond to the crest of the ramp anticline.

The interpreted magnitude of translation of the Jones Valley thrust sheet is tested in a palinspastic restoration (Fig. 8C) by balancing two independent stratigraphic criteria. Seismic reflection profiles show a large mass, lacking in internally coherent reflectors, beneath the preserved frontal ramp of the Jones Valley thrust fault (Thomas and Bayona, 2005; Thomas, 2007). A well along strike to the northeast and additional seismic reflection profiles indicate that the subsurface mass is a ductile duplex (mushwad) of the shale-dominated Middle to lower Upper Cambrian Conasauga Formation (Thomas, 2001). Area balance of the mushwad palinspastically restores the thick Cambrian shale into the Birmingham basement graben, the geometry of which is documented in seismic reflection profiles (Fig. 8) (Thomas, 2001, 2007; Thomas and Bayona, 2005). The regionally persistent Upper Cambrian–Lower Ordovician Knox Group of massive carbonate rocks, the regionally dominant stiff layer in Appalachian structures, is anomalously thin, where most of the upper units are locally truncated at a regional unconformity beneath Middle–Upper Ordovician strata (Bayona and Thomas, 2003; Thomas and Bayona, 2005; Thomas, 2007). Systematic reconstruction along strike shows that the area of anomalously great truncation of the upper Knox Group restores palinspastically within the Birmingham graben, and mechanical modeling indicates that the excess erosion is a result of basement fault inversion during Taconic (Ordovician) tectonic loading (Bayona and Thomas, 2003). Successful area balancing of the thick Cambrian shale in the Birmingham graben and the comparable restoration of the truncated Knox Group within the graben are consistent with an 18 km displacement required to place the leading edge of the Jones Valley thrust sheet over the area of the thermal anomaly. The internally consistent geometry of the restoration is a strong test of the validity of the cross section.

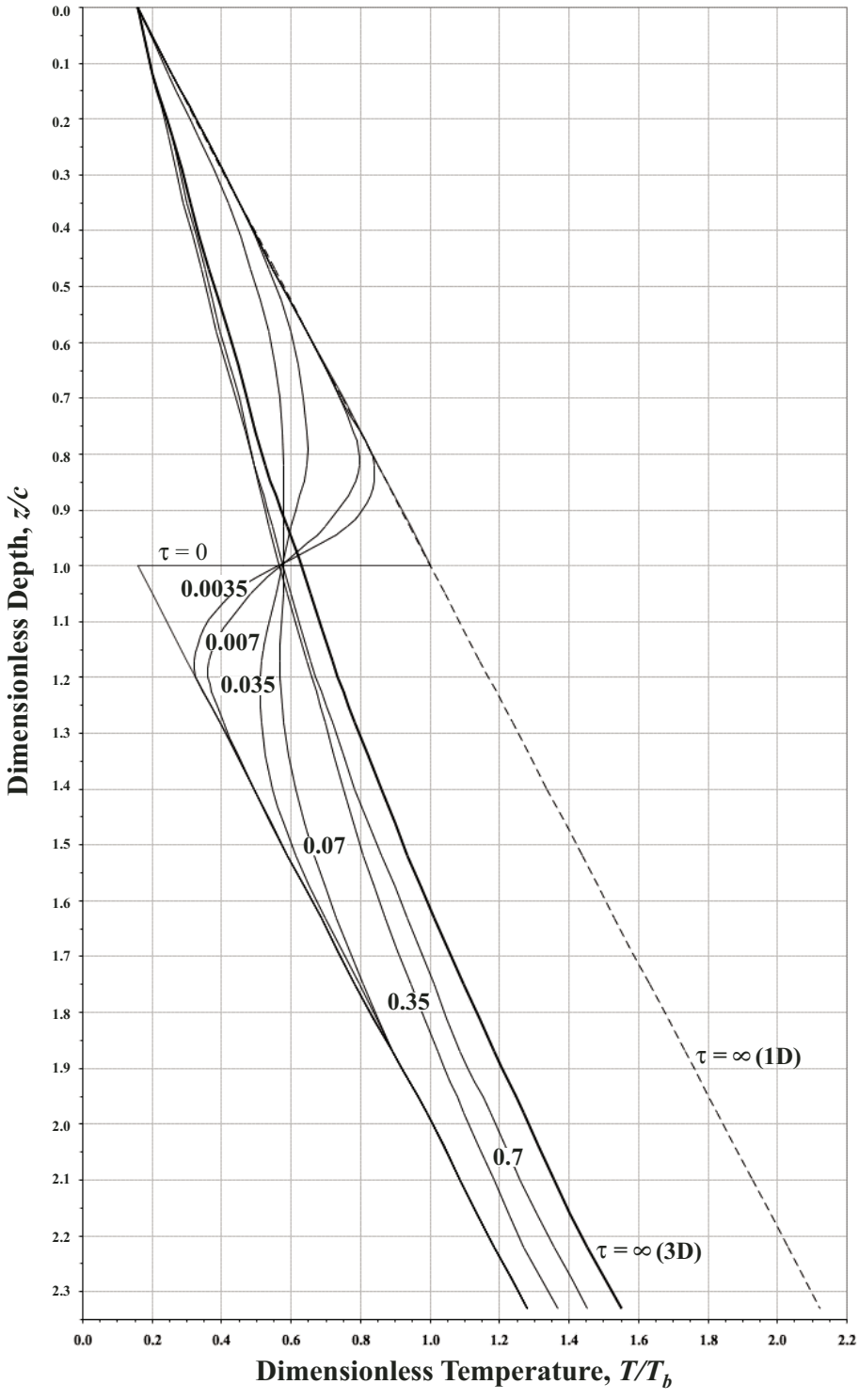

Figure 6. Dimensionless temperature T^* (= T/T_b, where T_b is the initial temperature at the top of the footwall) plotted against dimensionless depth (total depth below top of the thrust sheet divided by thickness of the thrust sheet) as a function of dimensionless time $\tau = \kappa t/c^2$, where κ is thermal diffusivity (10^{-6} m^2/s) (Turcotte and Schubert, 2002), t is time since thrust emplacement, and c is thrust-sheet thickness for the center of the thrust sheet. Also shown (dashed line) is the one-dimensional solution for vertical cooling at infinite time (i.e., the normal reestablished geotherm). For three-dimensional cooling, the geotherm is never fully reestablished and reaches a steady state at ~2 m.y. A plot of $\tau = 3.5$ is (slightly lower than but) indistinguishable at the scale of this plot from $\tau = \infty$.

Along-Strike Limits of the Thermal Anomaly; Jones Valley Lateral Ramps

Northwest of the Jones Valley fault, the Sequatchie anticline is a detachment anticline along the foreland limit of the regional décollement, marking the front of the Appalachian thrust belt along the southeast side of the Black Warrior foreland basin (Fig. 1). The trailing limb of the Sequatchie anticline defines the Coalburg syncline, the southeast limb of which is steeply upturned to overturned.

The thrust-belt structures show abrupt along-strike changes in structural profile across the Bessemer transverse zone, which is a cross-strike alignment of cross-strike links (lateral ramps, transverse faults, displacement transfers, and displacement gradients) in thrust-belt structures (Thomas, 1990; Thomas and Bayona, 2005). Northeast of the Bessemer transverse zone, the Opossum Valley fault is a leading splay of the Jones Valley fault (Figs. 1 and 2), and the steep upturn of the southeast limb of the Coalburg syncline is in the footwall of the Opossum Valley thrust sheet, which forms the footwall of the Jones Valley fault. Southwestward along strike across the Bessemer transverse zone, the Sequatchie anticline ends through a displacement gradient, and beyond the southwest end of the anticline, the Coalburg syncline merges with the Black Warrior foreland basin. The Opossum Valley thrust sheet ends southwestward in the Bessemer transverse zone at a lateral ramp in the Jones Valley footwall (Fig. 2). The Blue Creek fault extends along strike southwestward from the lateral ramp at the southwest end of the Opossum Valley thrust sheet; however, the Blue Creek fault passes southwestward into a blind fault beneath the low-amplitude Blue Creek anticline and a trailing syncline. The structural geometry of the Blue Creek anticline-syncline pair reflects an upper-level flat-and-ramp geometry of the Blue Creek fault (Fig. 8). The steep upturn of the trailing limb of the Coalburg syncline in the footwall of the Opossum Valley fault is transferred sinistrally via a lateral ramp to the trailing limb of the Blue Creek syncline in the Blue Creek hanging wall, which is in the footwall of the Jones Valley fault. The steep to overturned southeast limb of the Blue Creek syncline includes a folded southeast-verging backthrust. The Jones Valley fault cuts southwestward across the Opossum Valley lateral ramp onto the steep upturned trailing limb of the Blue Creek syncline in the Blue Creek thrust sheet (Fig. 2). The steeply upturned southeast limb of the Blue Creek syncline and the structurally comparable southeast limb of the Coalburg syncline represent the folded footwalls of the Jones Valley

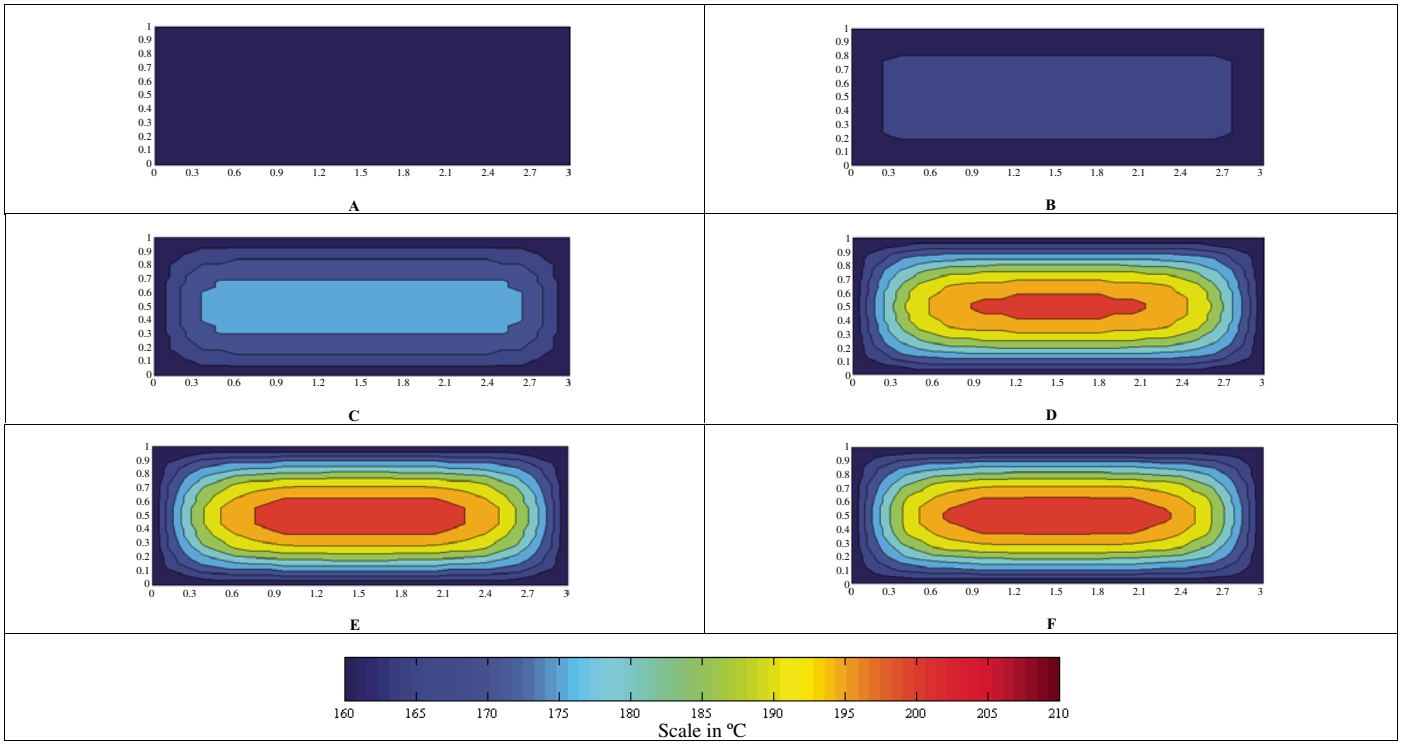

Figure 7. Temperature distribution at a depth of 3 km in the footwall after emplacement of a 3-km-thick thrust sheet with dimensions of 10 × 30 km for times of (A) 0, (B) 10^4, (C) 5×10^4, (D) 10^5, (E) 5×10^5, and (F) 10^6 yr after emplacement of the thrust sheet (units of horizontal dimensions = 10 km). Comparing Figure 7 with Figure 5, the thrust sheet cools laterally along the bounding thrust ramps: the leading hanging-wall frontal ramp, both hanging-wall lateral ramps, and the trailing hanging-wall fault-bend fold over the footwall frontal ramp. An oval thermal anomaly appears after ~10^5 yr (D), corresponding to a temperature of ~200 °C, in agreement with the observed vitrinite reflectance (coal rank) anomaly (Fig. 2).

fault and Opossum Valley fault, respectively. Because the trailing cutoff of the Opossum Valley thrust sheet is the leading cutoff of the Jones Valley fault, the lateral ramp at the southwest end of the Opossum Valley fault must have had a counterpart dextral lateral ramp in the now-eroded leading part of the Jones Valley thrust sheet. The dextral lateral ramp corresponds to the northeast end of the thermal anomaly (cf. Fig. 2 and Fig. 5).

Along strike southwestward, near where the Appalachian structures pass southwestward beneath postorogenic cover of the Gulf Coastal Plain, the trace of the Jones Valley fault describes an abrupt sinistral curve (Fig. 2), marking a sinistral lateral ramp. Across strike to the northwest, plunging folds indicate a similar lateral ramp in the Blue Creek fault, conforming to an Appalachian transverse zone approximately along the present eroded edge of the Gulf Coastal Plain (Surles and Thomas, 2006; Surles, 2007), here termed the Coastal Plain transverse zone (Figs. 1 and 2). The sinistral lateral ramp in the Jones Valley fault corresponds to the southwest end of the thermal anomaly.

Southeast Edge of the Thermal Anomaly; Jones Valley Footwall Frontal Ramp

The southeast (trailing) edge of the thermal anomaly corresponds to the present location of the Blue Creek anticline-syncline pair in the footwall of the Jones Valley fault and is ~8 km northwest of the presently exposed trace of the Jones Valley fault. Southeast of the anomaly, vitrinite reflectance values are at the background level (Fig. 2), consistent with a 3-km-thick cover. The Jones Valley fault ramps through the steeply upturned beds along the southeastern trailing limb of the Blue Creek syncline. The thermal values are consistent with a footwall flat approximately at the level of the Mary Lee coal across a flat structural shoulder between the steep upturn on the southeast and the shallow depression of the Blue Creek syncline on the northwest (Fig. 8). Emplacement of the Jones Valley thrust sheet over a flat approximately at the level of the Mary Lee coal results in negligible footwall stratigraphic cover and a 3-km-thick tectonic (thrust-sheet) cover. The northwest edge of the footwall flat is approximately at the Blue Creek anticline, which may have deflected the Jones Valley fault upward into a northwest-vergent footwall frontal ramp, accounting for the base of the southeastward gradient of the thrust-related thermal anomaly. The southeastern base of the southeastward gradient, ~8 km northwest of the present eroded trace of the Jones Valley fault, is interpreted to mark the base of a footwall frontal ramp where the fault cuts upsection in the footwall northwestward in the direction of transport from a stratigraphic level near the Mary Lee coal group (over the area of background thermal values) to a stratigraphic level ~3 km higher over the area of the thermal anomaly (Fig. 8). In that configuration, the southeastward gradient of the thermal anomaly corresponds in area to that of the southeast-dipping footwall frontal ramp.

Regional Distribution of Displacement on the Jones Valley Thrust Fault

Regionally, the Jones Valley fault ends northeastward along strike in the Harpersville transverse zone through a displacement gradient (Fig. 1) (Thomas and Bayona, 2005).

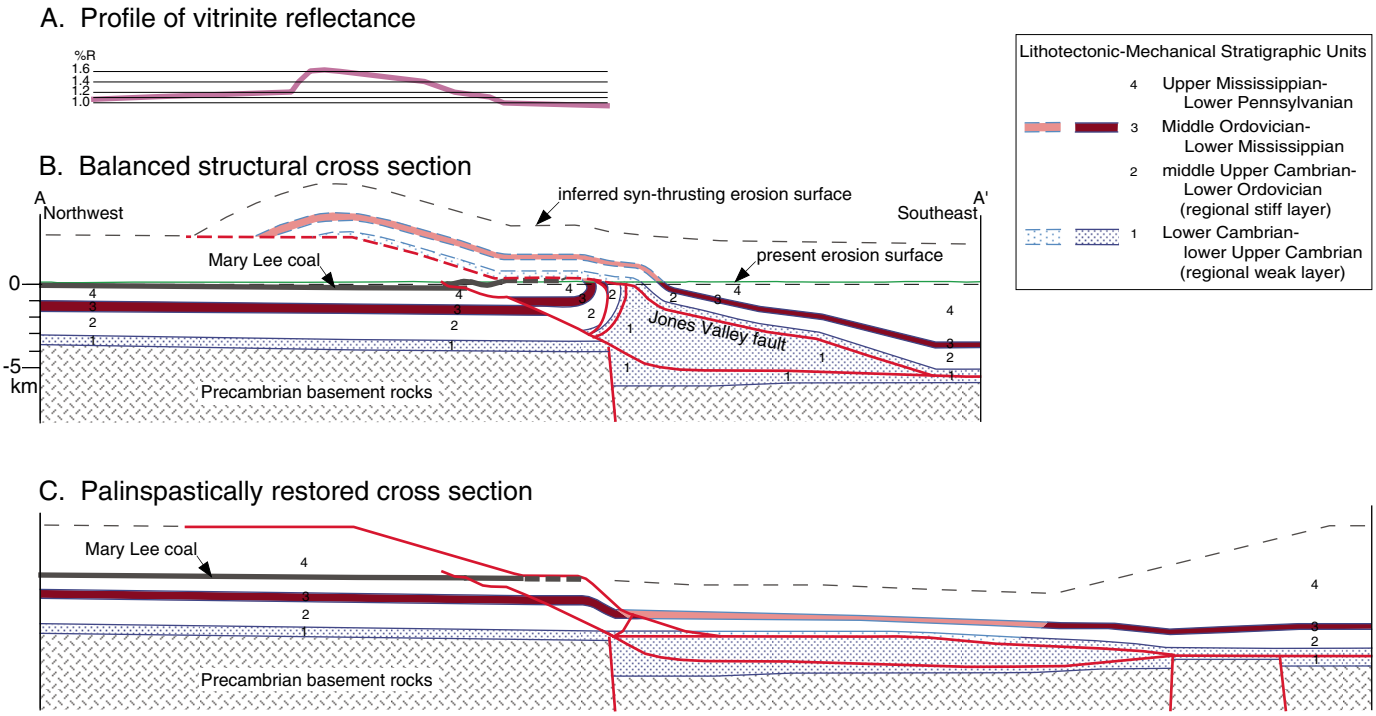

Figure 8. Balanced and palinspastically restored cross section (modified from Thomas and Bayona, 2005) across the vitrinite reflectance anomaly in the footwall of the Jones Valley fault. Line of cross section shown in Figure 2 (A' is southeast of the map area). (A) Profile of vitrinite reflectance from contour map in Figure 2 placed geographically with respect to the cross section. (B) Balanced structural cross section of Jones Valley fault based on outcrop geology, seismic reflection profiles, and drill-hole data (Thomas and Bayona, 2005; Thomas, 2007), and on detailed geologic mapping along the steep southeast limb of the Blue Creek syncline in the footwall of the Jones Valley fault (Brewer, 2004). Lithotectonic-mechanical stratigraphic units are from Thomas (2007). Dashed lines and pale shading above present erosion surface show interpreted restoration of eroded cover. (C) Palinspastic restoration of the structural cross section (adapted from Thomas and Bayona, 2005, and Thomas, 2007). Dashed lines and pale shading show eroded cover as in B.

From zero displacement at the northeast end, displacement increases southwestward along strike of the Jones Valley fault; however, because the leading hanging-wall cutoffs have been eroded, the amount of thrust translation has not been quantified. Lateral ramps at the Bessemer and Coastal Plain transverse zones bound a leading salient of the Jones Valley thrust sheet; however, the leading part has been eroded. The thermal anomaly, which is documented by vitrinite reflectance (Fig. 2), shows the original extent of the Jones Valley thrust sheet, thereby quantifying the magnitude of thrust translation. The Jones Valley fault may have a classic bow-and-arrow trace and thrust displacement, decreasing to zero in both directions along strike from a maximum of ~18 km at the thermal anomaly.

DISCUSSION AND CONCLUSIONS

Crustal thickening as a result of thrusting in orogenic belts is recognized as an important cause of regional metamorphism, and thermal models of thrust belts have provided valuable insight into the interplay between tectonics and metamorphism (e.g., Oxburgh and Turcotte, 1974; Chamberlain and England, 1985; Karabinos and Ketcham, 1988; Spear et al., 1990). To date, most thermal models have been based on heat conduction in one or two dimensions for a thrust sheet of infinite horizontal extent. Two-dimensional modeling of thrust sheets in the horizontal and vertical directions shows that the time-temperature history varies considerably with the lateral position within the thrust sheet (Karabinos and Ketcham, 1988; Shi and Wang, 1987; Huerta and Rodgers, 2006). In this study, we use a three-dimensional heat conduction model to evaluate simultaneous vertical and two-dimensional horizontal heat transport in a rectangular thrust sheet. The three-dimensional model reproduces both the magnitude and the oval shape of anomalously high coal rank parallel to the thrust front in the southern Appalachians. Thickness and extent of the Jones Valley thrust sheet from the thermal model are consistent with balanced and restored cross sections based on geologic data. A thrust sheet ~3 km thick was emplaced ~18 km onto the foreland over the thermal anomaly. With these initial and boundary conditions, a solution to the three-dimensional heat conduction equation reproduces the magnitude and shape of the thermal anomaly in a time interval of 100–500 k.y. An important result of the three-dimensional model is that the geotherm in the hanging wall or footwall is never fully reestablished even after long times, because of lateral heat loss.

Lateral ramps are recognized as important features of thrust sheets. The three-dimensional thermal evolution of both the hanging wall and the footwall in thrust systems is distinct from that predicted by one-dimensional models; a three-dimensional model predicts less heating of the footwall because of horizontal heat loss across bounding lateral ramps. Horizontal cooling across ramps bounding thrust sheets may be an important orogenic cooling process, and may partly explain the paucity of thrust-related heat anomalies in the geologic record.

APPENDIX: SOLUTION PROCEDURE

We solve the 3D thermal diffusion equation to compute the temperature distribution, $T(x,y,z,t)$:

$$\nabla^2 T = \frac{\partial^2 T}{\partial x^2} + \frac{\partial^2 T}{\partial y^2} + \frac{\partial^2 T}{\partial z^2} = \frac{1}{\kappa}\frac{\partial T}{\partial t},$$

in the domain: $[0 \le x \le a; 0 \le y \le b; 0 \le z \le (1+f)c]$, (1a)

where T is temperature, x and y are orthogonal horizontal coordinates, z is depth (vertical direction and positive downward), κ is thermal diffusivity, t is time, a and b are the orthogonal horizontal dimensions of the thrust sheet, c is the thickness of the thrust sheet, and $(1+f)$ is the ratio of thickness in the footwall underlying the thrust sheet to that of the thrust sheet.
The boundary conditions are:

$$T_{(x=0)} = T_{(x=a)} = T_{(y=0)} = T_{(y=b)} = T_0 + \lambda(z-c)H(z-c) \quad (1b)$$

and

$$T_{(z=0)} = T_0; \quad \left.\frac{\partial T}{\partial z}\right|_{[z=(1+f)c]} = \lambda, \quad (1c)$$

where λ is the geothermal gradient.
The initial condition is:

$$T_{(t=0)} = T_0 + \lambda[zH(z) - cH(z-c)], \quad (1d)$$

where $H(z)$, the Heaviside or step function, is given by:

$$H(z) = 0 \text{ for } z < 0$$
$$= 1 \text{ for } z \ge 0, \quad (2)$$

where we assume that the z-coordinate is positive downward. In order to solve the partial differential equation defined by equation 1 analytically, we need homogeneous boundary conditions. This can be easily accomplished by the transformation:

$$u(x,y,z,t) = T(x,y,z,t) - [T_0 + \lambda(z-c)H(z-c)], \quad (3a)$$

which leads to

$$\frac{\partial}{\partial z}[u(x,y,z,t)] = \frac{\partial}{\partial z}[T(x,y,z,t)] - \lambda H(z-c) - \lambda(z-c)\frac{\partial}{\partial z}[H(z-c)]. \quad (3b)$$

The last term of equation 3b is the geothermal gradient multiplied by the Dirac-Delta function, $\delta(z-c)$. Therefore, equation 3b can be rewritten as:

$$\frac{\partial}{\partial z}[u(x,y,z,t)] = \frac{\partial}{\partial z}[T(x,y,z,t)] - \lambda H(z-c) - \lambda(z-c)\delta(z-c). \quad (3c)$$

Substituting equations 3a and 3c into equation 1, the diffusion equation is transformed into:

$$\nabla^2 u = \frac{\partial^2 u}{\partial x^2} + \frac{\partial^2 u}{\partial y^2} + \frac{\partial^2 u}{\partial z^2} = \frac{1}{\kappa}\frac{\partial u}{\partial t} + Q(z), \quad (4a)$$

with homogeneous boundary conditions:

$$u_{(x=0)} = u_{(x=a)} = u_{(y=0)} = u_{(y=b)} = 0 \quad (4b)$$

$$u_{(z=0)} = 0; \quad \left.\frac{\partial u}{\partial z}\right|_{[z=(1+f)c]} = 0 \quad (4c)$$

and a transformed initial condition:

$$u_{(t=0)} = \lambda z\,[H(z) - H(z-c)] = \Phi(z). \quad (4d)$$

A pseudo-source term, $Q(z)$, now appears in the diffusion equation (equation 4a), given by:

$$Q(z) = -\lambda\left\{2\delta(z-c) + (z-c)\frac{\partial^2}{\partial z^2}[H(z-c)]\right\}. \quad (4e)$$

Although the last term of equation 4e is not defined (because it is the derivative of the Dirac-Delta function), the Fourier coefficients of the series solution of equation 4a are all defined, and can be exactly computed. This is because the differential operator is cancelled by the integral operator during Fourier coefficient determination, giving back the Dirac-Delta function (see below). Equation 4 can be solved using the method of eigen-function expansions. Assume that the solution is the summation of an infinite series of eigen-function products, having the form:

$$u(x,y,z,t) = \sum_{m=1}^{\infty}\sum_{n=1}^{\infty}\sum_{q=0}^{\infty} A_{mnq}(t)\,Sin\left(\tfrac{m\pi x}{a}\right)Sin\left(\tfrac{n\pi y}{b}\right)Cos\left\{\left[\tfrac{(2q+1)\pi}{2}\right]\left[1-\tfrac{z}{(1+f)c}\right]\right\}. \quad (5a)$$

Equation 5a satisfies all the boundary conditions of equation 4. We further assume that both the initial condition $\Phi(z)$ and the source term $Q(z)$ can be similarly expressed, i.e.,

$$u(x,y,z,0) \equiv \Phi(z) = \sum_{m=1}^{\infty}\sum_{n=1}^{\infty}\sum_{q=0}^{\infty} \phi_{mnq}\,Sin\left(\tfrac{m\pi x}{a}\right)Sin\left(\tfrac{n\pi y}{b}\right)Cos\left\{\left[\tfrac{(2q+1)\pi}{2}\right]\left[1-\tfrac{z}{(1+f)c}\right]\right\} \quad (5b)$$

and
$$Q(z) = \sum_{m=1}^{\infty}\sum_{n=1}^{\infty}\sum_{q=0}^{\infty} q_{mnq}\,Sin\left(\tfrac{m\pi x}{a}\right)Sin\left(\tfrac{n\pi y}{b}\right)Cos\left\{\left[\tfrac{(2q+1)\pi}{2}\right]\left[1-\tfrac{z}{(1+f)c}\right]\right\}. \quad (5c)$$

The Fourier coefficients for Φ are given by:

$$\phi_{mnq} = \tfrac{8}{abc(1+f)}\int_0^a\int_0^b\int_0^c \Phi(z)\,Sin\left(\tfrac{m\pi x}{a}\right)Sin\left(\tfrac{n\pi y}{b}\right)Cos\left\{\left[\tfrac{(2q+1)\pi}{2}\right]\left[1-\tfrac{z}{(1+f)c}\right]\right\}dxdydz. \quad (6a)$$

Substituting equation 4d into equation 6a, the Fourier coefficients for the eigen-function expansion of Φ are:

$$\phi_{mnq} = \tfrac{16\lambda c(1+f)[1-Cos(m\pi)][1-Cos(n\pi)]}{mn(2q+1)\pi^3}\left\{\tfrac{2}{\pi(2q+1)}Cos\left[\tfrac{(2q+1)f}{2(1+f)}\pi\right] - \tfrac{1}{1+f}Sin\left[\tfrac{(2q+1)f}{2(1+f)}\pi\right]\right\}. \quad (6b)$$

Similarly, substituting equation 4e into equation 6a (with Φ replaced by Q), the Fourier coefficients for the eigen-function expansion of Q are:

$$q_{mnq} = -\tfrac{8\lambda[1-Cos(m\pi)][1-Cos(n\pi)]}{mnc(1+f)\pi^2}\left\{Cos\left[\tfrac{(2q+1)f}{2(1+f)}\pi\right]\right\}. \quad (7)$$

Both ϕ_{mnq} and q_{mnq} are non-zero only if both m and n are odd. Substituting equations 5a and 5b into equation 4a, we obtain a first-order ordinary differential equation for the Fourier coefficients for u: $A_{mnq}(t)$, in terms of the Fourier coefficients for Q and Φ. The solution to this ordinary differential equation is:

$$A_{mnq}(t) = \frac{q_{mnq}}{\alpha_{mnq}^2}\left(1 - e^{-\kappa\alpha_{mnq}^2 t}\right) + \phi_{mnq}e^{-\kappa\alpha_{mnq}^2 t}, \quad (8a)$$

where α_{mnq} is given by:

$$\alpha_{mnq}^2 = \pi^2\left\{\left(\frac{m}{a}\right)^2 + \left(\frac{n}{b}\right)^2 + \left[\frac{2q+1}{2(1+f)c}\right]^2\right\}. \quad (8b)$$

Thus the Fourier coefficients for u can be directly computed by substituting equations 6, 7, and 8b into equation 8a. A Fortran 90 code was written to compute the series summation solution efficiently. At each time step, the temperature distributions corresponding to 6 depths between 1 km and 6 km, at 1 km intervals, were estimated over a computational grid of 51 × 26 nodes. In addition, the temperature profile along a vertical line perpendicular to the thrust plane, passing through the center of the thrust sheet ($x = a/2$, $y = b/2$), was computed at a depth resolution of ~50 m (141 nodes). To test for convergence of the solution, as well as accuracy,

partial sums were estimated at a few sample locations using a spreadsheet. These partial sums were computed, using successively larger numbers of terms, until the solution converged to within 0.1 °C. The series summation converged after ~100,000 terms. In order to be conservative, however, the solutions presented here were computed using more than 250,000 non-zero terms (i.e., for m = 1 to 100, n = 1 to 100, and q = 0 to 100).

ACKNOWLEDGMENTS

Acknowledgment is made to the donors of the Petroleum Research Fund (38965), administered by the American Chemical Society, for support of this research. Jack Pashin provided the graphics files for Figure 3 and the volatile-matter contour map in Figure 2, as well as helpful advice on sample selection and a review of a draft of the manuscript. Richard Carroll provided numerous core samples from boreholes. Brian Cook, Liz Dodson, and Carrie Kidd assisted in the compilation and computation for the tables and Figure 4. We thank John Costain, Rick Groshong, Bob Hatcher, and Sid Jones for helpful reviews of the manuscript.

REFERENCES CITED

Barker, C.E., and Goldstein, R.H., 1990, Fluid-inclusion technique for determining maximum temperature in calcite and its comparison to the vitrinite reflectance geothermometer: Geology, v. 18, p. 1003–1006, doi: 10.1130/0091-7613(1990)018<1003:FITFDM>2.3.CO;2.

Bayona, G., and Thomas, W.A., 2003, Distinguishing fault reactivation from flexural deformation in the distal stratigraphy of the peripheral Blountian foreland basin, southern Appalachians, USA: Basin Research, v. 15, p. 503–526, doi: 10.1046/j.1365-2117.2003.00217.x.

Blackwell, D.D., and Steele, J.L., 1989, Thermal conductivity of sedimentary rocks—Measurement and significance, *in* Naeser, N., and McCulloh, T., eds., Thermal history of sedimentary basins: New York, Springer, p. 13–36.

Bott, H.P., 1982, The interior of the Earth: Its structure, constitution and evolution (second edition): New York, Elsevier, 396 p.

Boyer, S.E., and Elliott, D., 1982, Thrust systems: American Association of Petroleum Geologists Bulletin, v. 66, p. 1196–1230.

Brewer, M.C., 2004, Geometric and kinematic evolution of the Bessemer transverse zone, Alabama Alleghanian thrust belt [Ph.D. thesis]: Lexington, University of Kentucky, 235 p.

Bustin, R.M., 1983, Heating during thrust faulting in the Rocky Mountains: Friction or fiction: Tectonophysics, v. 95, p. 309–328, doi: 10.1016/0040-1951(83)90075-6.

Carroll, R.E., Pashin, J.C., and Kugler, R.L., 1993, Burial history and source-rock characteristics of Upper Devonian through Pennsylvanian strata, Black Warrior basin, Alabama: Alabama Geological Survey Circular 187, 13 p.

Cercone, K.R., Deming, D., and Pollack, H.N., 1996, Insulating effect of coals and black shales in the Appalachian basin, western Pennsylvania: Organic Geochemistry, v. 24, p. 243–249, doi: 10.1016/0146-6380(96)00021-6.

Chamberlain, P.C., and England, P.C., 1985, The Acadian history of the Merrimack synclinorium in New Hampshire: Journal of Geology, v. 93, p. 593–602.

Culbertson, W.C., 1964, Geology and coal resources of the coal-bearing rocks of Alabama: U. S. Geological Survey Bulletin 1182-B, 79 p.

Furlong, K.P., and Edman, J.D., 1984, Graphic approach to determination of hydrocarbon maturation in overthrust terrains: American Association of Petroleum Geologists Bulletin, v. 68, p. 1818–1824.

Goldhaber, M.B., Lee, R.C., Hatch, J.R., Pashin, J.C., and Treworgy, J., 2003, Role of large-scale fluid flow in subsurface arsenic enrichment, *in* Welch, A.H., and Stollenwerk, K.G., eds., Arsenic in ground water: Geochemistry and occurrence: Dordrecht, Kluwer, p. 127–176.

Hines, R.A., Jr., 1988, Carboniferous evolution of the Black Warrior foreland basin, Alabama and Mississippi [Ph.D. thesis]: Tuscaloosa, University of Alabama, 231 p.

Hower, J.C., 1978, Anisotropy of vitrinite reflectance in relation to coal metamorphism for selected United States coals [Ph.D. thesis]: State College, Pennsylvania State University, 339 p.

Huerta, A.D., and Rodgers, D.W., 2006, Constraining rates of thrusting and erosion: Insights from kinematic thermal modeling: Geology, v. 34, p. 541–544, doi: 10–1130/G22421.1.

Karabinos, P., and Ketcham, R., 1988, Thermal structure of active thrust belts: Journal of Metamorphic Geology, v. 6, p. 559–570, doi: 10.1111/j.1525-1314.1988.tb00440.x.

Laubscher, H.P., 1985, Large-scale thin-skinned thrusting in the southern Alps: Geological Society of America Bulletin, v. 96, p. 710–718, doi: 10.1130/0016-7606(1985)96<710:LTTITS>2.0.CO;2.

O'Hara, K., 2004, Paleo-stress estimates on ancient seismogenic faults based on frictional heating of coal: Geophysical Research Letters, v. 31, L03601, doi: 10.1029/2003GL018890.

O'Hara, K., Hower, J.C., and Rimmer, S.M., 1990, Constraints on the emplacement and uplift history of the Pine Mountain thrust sheet, eastern Kentucky: Evidence from coal rank trends: Journal of Geology, v. 98, p. 43–51.

O'Hara, K., Kanda, R.V., and Thomas, W.A., 2006, Thermal footprint of an eroded thrust sheet in the southern Appalachian Black Warrior basin, Alabama, USA: Geological Society of America Abstracts with Programs, v. 38, no. 3, p. 7.

Osborne, W.E., Szabo, M.W., Neathery, T.L., and Copeland, C.W., Jr., 1988, Geologic map of Alabama northeast sheet: Alabama Geological Survey Special Map 220, scale 1:250,000.

Oxburgh, E.R., and Turcotte, D.L., 1974, Thermal gradients and regional metamorphism in overthrust terrains with special reference to the eastern Alps: Schweizerische Mineralogische und Petrographische Mitteilungen, v. 56, p. 641–662.

Pashin, J.C., 2004, Cyclothems of the Black Warrior basin in Alabama: Eustatic snapshots of foreland basin tectonism: American Association of Petroleum Geologists Studies in Geology 51, p. 199–217.

Pashin, J.C., 2005, Coalbed methane exploration in thrust belts: Experience from the southern Appalachians, USA: Tuscaloosa, Alabama, University of Alabama, College of Continuing Studies, 2005 International Coalbed Methane Symposium Proceedings, paper 0519, 14 p.

Pashin, J.C., and Hinkle, F., 1997, Coalbed methane in Alabama: Alabama Geological Survey Circular 192, 71 p.

Pashin, J.C., Carroll, R.E., Hatch, J.R., and Goldhaber, M.B., 1999, Mechanical and thermal control of cleating and shearing in coal: Examples from the Alabama coalbed methane fields, USA, *in* Mastalerz, M., Glickson, M., and Golding, S., eds., Coalbed methane: Scientific, environmental and economic evaluation: Dordrecht, Kluwer, p. 305–328.

Pashin, J.C., Carroll, R.E., Groshong, R.H., Jr., Raymond, D.E., McIntyre, M.R., and Payton, J.W., 2004, Geologic screening criteria for sequestration of CO_2 in coal: Quantifying potential of the Black Warrior coalbed methane fairway, Alabama: U.S. Department of Energy, National Technology Laboratory, contract DE-FC26–00NT40927 Final Technical Report, 254 p.

Pashin, J.C., McIntyre, M.R., Carroll, R.E., Groshong, R.H., Jr., and Bustin, R.M., 2008, Carbon sequestration and enhanced recovery potential of mature coalbed methane reservoirs in the Black Warrior basin, *in* Grobe, M., et al., eds., Geological carbon sequestration—State of the science: American Association of Petroleum Geologists Studies in Geology 59 (in press).

Pitman, J.K., Pashin, J.C., Hatch, J.R., and Goldhaber, M.B., 2003, Origin of minerals in joint and cleat systems of the Pottsville Formation, Black Warrior basin, Alabama: Implications for coalbed methane generation and production: American Association of Petroleum Geologists Bulletin, v. 87, p. 713–731.

Price, R.A., 1988, The mechanical paradox of large overthrusts: Geological Society of America Bulletin, v. 100, p. 1898–1908, doi: 10.1130/0016-7606(1988)100<1898:TMPOLO>2.3.CO;2.

Rich, J.L., 1934, Mechanics of low-angle overthrust faulting as illustrated by Cumberland thrust block, Virginia, Kentucky and Tennessee: American Association of Petroleum Geologists Bulletin, v. 18, p. 1584–1596.

Shi, Y., and Wang, C., 1987, Two-dimensional modeling of the P-T-t paths of regional metamorphism in simple overthrust terrains: Geology, v. 15, p. 1048–1051, doi: 10.1130/0091-7613(1987)15<1048:TMOTPP>2.0.CO;2.

Singer, J.M., and Tye, R.P., 1979, Thermal, mechanical and physical properties of selected bituminous coals and cokes: U.S. Bureau of Mines Report of Investigations 8364, p. 1–37.

Spear, F.S., Hickmott, D.D., and Selverstone, J., 1990, Metamorphic consequences of thrust emplacement, Fall Mountain, New Hampshire: Geological Society of America Bulletin, v. 102, p. 1344–1360, doi: 10.1130/0016-7606(1990)102<1344:MCOTEF>2.3.CO;2.

Surles, D.M., 2007, Interactions between structures in the Appalachian and Ouachita foreland beneath the Gulf Coastal Plain [Ph.D. thesis]: Lexington, University of Kentucky, 145 p.

Surles, M., and Thomas, W.A., 2006, The Appalachian thrust belt beneath the cover of the Mesozoic-Cenozoic coastal plain in western Alabama and eastern Mississippi: Geological Society of America Abstracts with Programs, v. 38, no. 3, p. 7.

Sweeney, J.J., and Burnham, A.K., 1990, Evaluation of a simple model of vitrinite reflectance based on chemical kinetics: American Association of Petroleum Geologists Bulletin, v. 74, p. 1559–1570.

Szabo, M.W., Osborne, W.E., and Copeland, C.W., Jr., 1988, Geologic map of Alabama northwest sheet: Alabama Geological Survey Special Map 220, scale 1:250,000.

Telle, W.R., Thompson, D.A., Lottman, L.K., and Malone, P.G., 1987, Preliminary burial-thermal history investigations of the Black Warrior basin: Implications for coal-bed methane and conventional hydrocarbon development: Tuscaloosa, Alabama, Coalbed Methane Symposium Proceedings, p. 37–50.

Thomas, W.A., 1988, The Black Warrior basin, *in* Sloss, L.L., ed., Sedimentary cover—North American craton: U.S.: Boulder, Colorado, Geological Society of America, The Geology of North America, v. D-2, p. 471–492.

Thomas, W.A., 1990, Controls on locations of transverse zones in thrust belts: Eclogae Geologicae Helvetiae, v. 83, p. 727–744.

Thomas, W.A., 2001, Mushwad: Ductile duplex in the Appalachian thrust belt in Alabama: American Association of Petroleum Geologists Bulletin, v. 85, p. 1847–1869.

Thomas, W.A., 2007, Role of the Birmingham basement fault in thin-skinned thrusting of the Birmingham anticlinorium, Appalachian thrust belt in Alabama: American Journal of Science, v. 307, p. 46–62, doi: 10.2475/01.2007.03.

Thomas, W.A., and Bayona, G., 2002, Palinspastic restoration of the Anniston transverse zone in the Appalachian thrust belt, Alabama: Journal of Structural Geology, v. 24, p. 797–826, doi: 10.1016/S0191-8141(01)00117-1.

Thomas, W.A., and Bayona, G., 2005, The Appalachian thrust belt in Alabama and Georgia: Thrust-belt structure, basement structure, and palinspastic reconstruction: Alabama Geological Survey Monograph 16, 48 p., 2 plates.

Turcotte, D.L., and Schubert, G., 2002, Geodynamics (second edition): Cambridge, Cambridge University Press, 456 p.

Winston, R.B., 1990a, Vitrinite reflectance of Alabama's bituminous coal: Alabama Geological Survey Circular 139, 54 p.

Winston, R.B., 1990b, Preliminary report on coal quality trends in upper Pottsville Formation coal groups and their relationship to coal resource development, coalbed methane occurrence, and geologic history in the Warrior coal basin, Alabama: Alabama Geological Survey Circular 152, 53 p.

Manuscript Received 7 December 2007
Revised Manuscript Received 8 May 2008
Manuscript Accepted 14 May 2008